Noncontact Laser Ultrasound for Biomedical Imaging Applications

Robert W. Haupt, Charles M. Wynn, Matthew R. Johnson, Jonathan R. Fincke, Xiang Zhang,

Brian W. Anthony, and Anthony E. Samir

Lincoln Laboratory, the MIT Medical Electronic Device Realization Center, and Massachusetts General Hospital are developing an optical system that acquires ultrasound images of the human body's interior without touching the patient. The noncontact laser ultrasound (N-CLUS) images tissue and bone and measures their elastographic properties from a distance of several inches to meters from the patient. The N-CLUS can be automated to provide a repeatable fixed frame of reference and could compete with magnetic resonance and computed tomography while reducing the system cost, complexity, and health risks. Such a system would expand the role of accurate imaging capabilities inside and outside the hospital center.

» **Ultrasound is an ideal method used in** medical practice to image the human body's interior [1]. It is portable, inexpensive, and causes no harmful biological effects in the patient while producing images with excellent resolution. Moreover, the ultrasound capability can measure blood flow and provides information about the mechanical properties (elastography) of tissue, organs, and bone. Despite ultrasound's advantages, magnetic resonance imaging (MRI) and computed tomography (CT) are the dominant imaging methods in medicine even though they impose health risks and are greater than ultrasound systems in size, cost, and complexity. Ultrasound would be ubiquitous in all of medicine but for one central problem: the need for transducer-to-skin contact necessitates manual device operation, which introduces variability between measurements, reduces the availability of ultrasound systems to patients, and increases the cost of the system. Manual transducer operation has been a central limitation of medical ultrasound for 50 years.

Contact transducers suffer problems in irreproducibility of measurements because each individual operator spontaneously chooses the transducer's look angle and application pressure to couple and transmit ultrasonic waves into the patient. These spontaneous actions differ greatly between measurements and between different medical operators, resulting in interoperator variability. This variability causes unpredictable signal and image distortion. More specifically, the localized tissue's mechanical properties change because of compaction differences in the vicinity of the transducer. Compaction occurs when the operator pushes the transducers onto

the patient's skin to achieve signal coupling, causing the skin to bunch together or distort. The unevenness of the skin causes variable ultrasonic wave velocities and travel paths. Theses numerous variations distort the clarity of the measured features' geometry and dimensions at depth as displayed in the resulting ultrasound image. Because of the variability between measurements, repeat measurements can miss important changes in tissue features over time. Ultrasound is further weakened by the lack of a fixed frame of reference to register the image location. Thus, MRI and CT are typically mandated over ultrasound because these methods provide fixed, gantry-mounted transmit-and-receive systems that enable spatially reproducible images and permit more accurate comparison of disease states over time.

Interoperator variability greatly limits ultrasound applications. For example, the American Thyroid Association's ultrasound guidelines require an increase in thyroid nodule volume of more than 50 percent—or an increase of more than 20 percent in two or more measured dimensions—before a biopsy can be recommended [2]. Large increases in nodule size are necessary before nodule growth can be confidently diagnosed because of the high interoperator variability associated with conventional ultrasound. The European Organization for Research and Treatment of Cancer and Response Evaluation Criteria in Solid Tumors' guidelines [3] do not permit the use of ultrasound tumor measurements for the follow-up of cancer because of high interoperator variability. Patients with cancer must be followed up with CT or MRI scans.

The advantages of three different medical imaging methods are compared in Table 1. The CT method offers high-resolution imaging capabilities that have been used for many years. The MRI method sets the standard for volumetric imaging inside the human body to detect and diagnose a variety of maladies in tissue, organs, the brain, and bone without the radiation risk of CT. Moreover, MRI techniques have evolved for new applications, such as tumor detection (elastography), in which anomalous voxels (3D pixels) in an MRI image indicate stiffer tissue masses that could be a sign of cancer. However, because MRI and CT systems are large, expensive, and require highly trained medical staff to operate, they are impractical for mass production and for many field-forward settings (locations outside hospital centers). A

fundamental drawback to MRI and CT is that they are only available to a small number of patients per day because measurement with these devices take a long time (30 to 60 minutes per patient) and because there are few units per hospital. There is great appeal in developing accurate imaging systems that combine the spatial reproducibility advantages of CT and MRI with the low-cost, portability, ease of operation, high-throughput, and low-toxicity advantages of medical ultrasound.

Appeal of Noncontact Laser Ultrasound

Noncontact laser ultrasound (N-CLUS) is designed to mitigate operator variability while providing a fixed-reference measurement capability [4]. Unlike contact transducers, laser ultrasound does not cause large-scale tissue compaction, and it also eliminates the variable of transducer look angle selection. Laser excitation and receive locations on the skin's surface can be revisited with spatial precision, permitting the system to monitor subtle changes in the geometry of measured features and the mechanical properties of tissue over time. Another advantage of laser ultrasound is that it does not necessitate contact with damaged or burned skin, painful regions, traumatized tissue, areas susceptible to infection and contamination, and areas awkward or difficult to reach. Standoff laser ultrasound can be directed with a mirror and is less likely to interfere with other medical procedures, such as surgery, compared to conventional ultrasound. With the proper development, N-CLUS medical imaging systems could potentially compete with MRI and CT as a lower-cost, portable, and health risk–free alternative. Such systems would expand the role of accurate imaging capabilities beyond the hospital center and enable numerous new medical ultrasound applications. We are currently receiving funding from the U.S. Army to develop N-CLUS for critical life-saving systems that are used to assess soldiers' injuries in field-forward environments. The MRI and CT methods are highly impractical for such environments because of their large weight, size, and power requirements.

The N-CLUS system generates an ultrasonic wave by first emitting short, high-peak-power infrared pulses from a Q-switched laser. The short pulses of optical energy reach the skin's surface and convert to mechanical energy via thermal expansion in the shallow layers of the

ROBERT W. HAUPT, CHARLES M. WYNN, MATTHEW R. JOHNSON, JONATHAN R. FINCKE, XIANG ZHANG, BRIAN W. ANTHONY, AND ANTHONY E. SAMIR

Table 1. The Pros and Cons of Magnetic Resonance Imaging and Computerized Tomography Are Compared to the Pros and Cons of Current Medical Ultrasound

TYPE OF IMAGING METHOD	PROS	CONS
MAGNETIC RESONANCE IMAGING (MRI) 	• High resolution • Safe • Fixed-reference gantry—enables time image progression monitoring	• Large, expensive, in-hospital • Danger from metal debris • Time-consuming • Uncomfortable for many patients—can require sedation in some cases
COMPUTERIZED TOMOGRAPHY (CAT SCAN) 	• High resolution • Fixed-reference gantry—enables time image progression monitoring	• Large, expensive, in-hospital • Weak on tissue contrasts • Radiation risk • Time-consuming • Uncomfortable for many patients—can require sedation in some cases
ULTRASOUND 	• High resolution • Portable, inexpensive • Safe • In-hospital and field-forward	• Image distortion from interobserver variability • No fixed reference • Impractical for time progression imaging in many applications
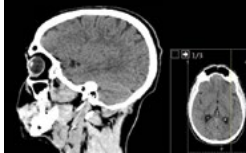
skin; then, the optically absorptive material of the skin rapidly deforms and launches a propagating mechanical wave response [5]. These processes are termed photoacoustic effects. From our studies, we found that long infrared wavelengths absorb rapidly in tissue (the wave attenuates in tissue depths of less than 1 millimeter) and create a consistent uniform acoustic source that generates a coherent broadband ultrasonic wave that propagates well into the far field within tissue (several inches there and back). We observed that this acoustic source is not influenced by skin pigment or topography, which

indicates that such a system could be used on any patient or skin condition. Finally, the mechanical/vibrational signature of the ultrasonic wave returning from inside the body is measured at the skin's surface with a laser Doppler vibrometer (LDV).

Research on noncontact acoustic and vibrational ultrasound has been ongoing for the past two decades [6–11]. Much of the focus has been on photoacoustic tomography (PAT), which is a popular method used in studies to image near-surface shallow capillaries in animal tissue. In PAT, pulsed infrared light penetrates

tissue and induces photoacoustic phenomena preferentially in chromophores (e.g., hemoglobin). Contact transducers then measure the emitted acoustic response. The PAT approach employs near-infrared wavelengths (700 to 900 nanometers) to maximize the penetration of light to the depth of interest and map optical absorptivity variations in tissue, such as blood vessels, with excellent spatial resolution. However, optical scatter severely limits the penetration of PAT to tissue depths of less than 1 centimeter. Recent studies have explored replacing contact transducers with an LDV as a sensing device to make the PAT system totally noncontact [10, 12]. However, for optical measurement systems to compete with practiced medical ultrasound, these systems need to generate acoustic waves in the frequency bands relevant to clinical ultrasound while being able to propagate to depths of several inches in the body. The laser system would need to operate within skin- and eye-safe laser powers and provide submillimeter resolution, an excellent signal-to-noise ratio (SNR), and rapid data acquisition times.

Operational Concept: Standoff N-CLUS Wave Generation with Laser Measurement

In the N-CLUS system, photoacoustic excitation is used in conjunction with an LDV to acquire ultrasonic waves without touching the patient's skin, as demonstrated in Figure 1. Photoacoustic phenomena develop from optical energy shaped in very short (picoseconds to nanoseconds) laser pulses that interact with an optically absorptive target surface, such as water or biological tissue, in which optical energy rapidly converts into heat [5, 15]. This nearly instantaneous heating creates a concentration of mechanical stress within the irradiated tissue patch. Because the tissue is no longer in mechanical equilibrium, the stress dissipates and generates a propagating acoustic wave into the tissue mass at a high frequency of approximately 1 megahertz.

Photoacoustic Phenomena Leading to Ultrasonic Wave Propagation in Tissue

Photoacoustic phenomena involve the conversion of optical energy into a localized pressure rise in biological tissue and are well described in the literature [6, 13–15]. The Gruneisen parameter, Γ, of tissue relates the initial pressure, p_0, to the light absorption in the expression

$$p_0 = \Gamma \mu_a F, \text{ where } \Gamma = \beta v_s^2 / C_p$$

where μ_a is the optical absorption coefficient of tissue, F is the local light fluence (optical intensity), β is the isobaric volume expansion coefficient, v_s^2 is the acoustic wave speed in tissue, and C_p is the specific heat of the tissue. The local pressure rise then results in acoustic wave propagation and is expressed below as a function of distance and time ($\boldsymbol{r}$, t).

$$\nabla^2 p(\mathbf{r},t) - \frac{1}{v_s^2}\frac{\partial^2 p(\mathbf{r},t)}{\partial t^2} = \frac{\beta}{C_p}\left[\mu_a + \Delta\mu_a(\mathbf{r})\right]\frac{\partial F(\mathbf{r},t)}{\partial t}$$

Photoacoustic phenomena and the process of ultrasonic wave propagation in biological tissue are explicitly derived and shown in detail in this article's Appendix.

Laser Doppler Vibrometry Sensitivity and Noise-Floor Components

To construct a fully noncontact laser ultrasound system, we used a heterodyne coherent laser radar (ladar) that acted as a vibrometer to measure the returning vibrational signals of ultrasonic waves emerging at the tissue's surface. In heterodyne detection, a signal of interest at a certain frequency is nonlinearly mixed with a reference local oscillator set at a nearby frequency. The desired output is the difference signal, which carries the information (amplitude, phase, and frequency modulation) of the original higher frequency signal. Optical photons are detected by their energy levels or by photon counting at the receiver and are proportional to the square of the electric field, thus forming a nonlinear event. When the local oscillator and the signal beams impinge together on a target surface, they mix, producing heterodyne beat frequencies.

The sensitivity performance of the laser Doppler vibrometer (LDV) is determined by its noise floor [16]. The noise floor is the level of unwanted signals, or noise, that a signal must surpass to be detected. The total noise floor is expressed below.

$$N_{\text{total}} = \sqrt{\left(N_{\text{shot}}\right)^2 + \left(N_{\text{speckle}}\right)^2 + \left(P, N_{\text{patient}}\right)^2}$$

where N is noise and P is platform.

ROBERT W. HAUPT, CHARLES M. WYNN, MATTHEW R. JOHNSON, JONATHAN R. FINCKE, XIANG ZHANG, BRIAN W. ANTHONY, AND ANTHONY E. SAMIR
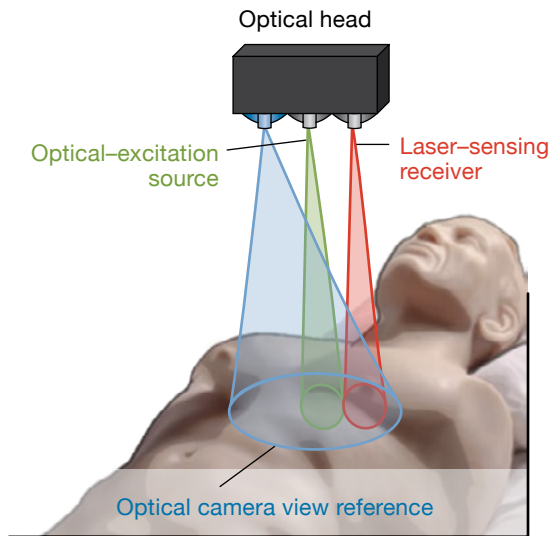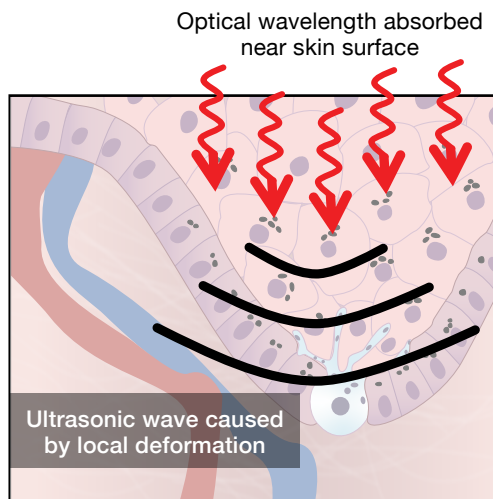
FIGURE 1. The diagrams demonstrate the notional N-CLUS system and how it acquires ultrasound images and measures mechanical properties of the body's interior without touching the subject. An optical head containing an excitation source and laser-sensing receiver is scanned over the body (a). The optical source emits pulsed infrared light, which enters the skin's surface layers and creates ultrasonic waves. The ultrasonic returns reflected off of the body's internal structures return to the surface of the skin and are measured with a laser Doppler vibrometer (b).
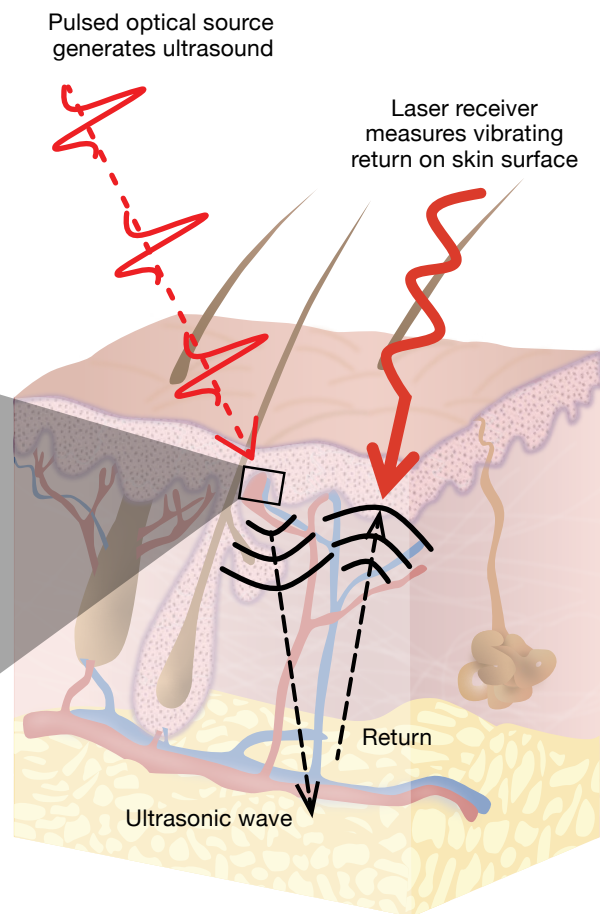
The shot noise is receiver-power limited, speckle noise is induced by motion, and platform and patient noise entail vibrations other than the ultrasonic waves of interest.

Shot noise depends on the number of photoelectrons received per second, ϕ_e (optical return from the vibrating tissue surface), over the vibrometer's demodulated bandwidth, and the shot noise in turn determines the received signal quality. The shot-noise spectrum of the surface particle velocity, $A_{v,sh}$, as a function of frequency, f, is proportional to the received returning photoelectrons for the transmit optical wavelength, λ, such that

$$A_{v,sh}(f) = \frac{f\lambda}{\sqrt{\phi e}}$$

As the bandwidth and desired frequency increase, the need for more photoelectrons also increases to maintain the desired noise floor. Increasing the LDV's fluence level provides more photoelectrons but runs the risk of exceeding skin- and eye-safety limits. The possibility of exceeding these limits is a critical concern in the development of a laser ultrasound system for patient skin exposure.

Speckle is the noise that occurs because of the distribution of optical scatterers on the tissue's surface that a laser beam encounters. For a diffuse surface, there are likely many optical scatterers (because of surface roughness) that reflect light back to the LDV. The speckle noise contribution to the laser-sensing system can be reduced by signal time integration with respect to the same realization of scatterers. The frequency-dependent speckle noise amplitude is shown below.

$$A_{v,sp}(f) = \lambda \sqrt{\frac{\pi f_{exc}^2}{12}} \sqrt{\frac{2\alpha}{\alpha^2 + (2\pi f)^2}}$$

where $\alpha = 2\pi f_{exc}$, and $f_{exc} = v_t/d$ (beam translation velocity on target over the beam diameter) is the exchange rate of the speckle pattern.

In terms of the LDV performance for ultrasonic measurements, the shot-noise contribution (at 1 megahertz) is anticipated to dominate the noise-floor sensitivity. When any motion from the patient is introduced to the system, speckle noise becomes a significant factor. Even subtle involuntary patient motion can produce significant fluctuations in the speckle realization and resultant noise floor. The design of a successful noncontact laser receiver critically depends on shot- and speckle-noise sources being sufficiently reduced to achieve a useful return SNR of the ultrasonic wave.

Lincoln Laboratory N-CLUS Demonstration System

We developed and built a proof-of-concept N-CLUS system to explore the phenomenology controlling optical absorption that generates useful ultrasonic waves and to demonstrate how to measure the waves without tissue contact. We explored the variety of elastic/ultrasonic waves that can be generated from a photoacoustic source, constructed images of tissue interiors with various systems, and compared these images to those produced by standard medical ultrasound. We explored the N-CLUS data-acquisition configurations that measure different ultrasonic wave types, such as longitudinal and shear waves in bone, which we analyzed to determine the bone's elastographic properties (elastic moduli) in vivo.

To provide the N-CLUS photoacoustic signal, we used several commercially available Q-switched laser sources, including a variable Continuum Panther optical parametric oscillator that drives the photoacoustic excitation source at prescribed optical wavelengths from the deep ultraviolet to near infrared, and a customized 1550-nanometer eye- and skin-safe power source. A fast steering mirror was used to position the laser beam onto the tissue sample's surface within submillimeter increments in the vertical and horizontal directions. A Polytec RSV-150 LDV was used as the receive system; its beam could be positioned with or without a mirror to the receiving location. The Polytec employs an eye- and skin-safe 1550-nanometer wavelength transmission at 10 milliwatts.

Return ultrasonic time series were collected on a Tektronix 200-megahertz digitizing scope and then recorded on a laptop computer. The excitation beam's location on the tissue sample was controlled by the fast steering mirror, which was positioned using an automated computer routine written in LabView software. Typically, scan lines are steered across the sample. A single scan line forms a 2D cross-sectional profile of the tissue sample. Multiple scan lines can be compiled to form a time image that is processed, converted to show depth, and migrated to display in 3D the physical layout of the tissue's interior features.

We employed a bistatic (i.e., set at different locations, as opposed to collocated) source and receiver geometry while varying the separation distance to accommodate standard seismic data processing algorithms that remove the effects of time distortion, such as normal move out and diffraction of point scatterers [18]. Normal move out corrections and time migration [17] are used to reduce the plotted cross-sectional data to obtain depth images of the tissue sample's interior. The N-CLUS experimental apparatus and measurement configuration are shown in Figure 2.
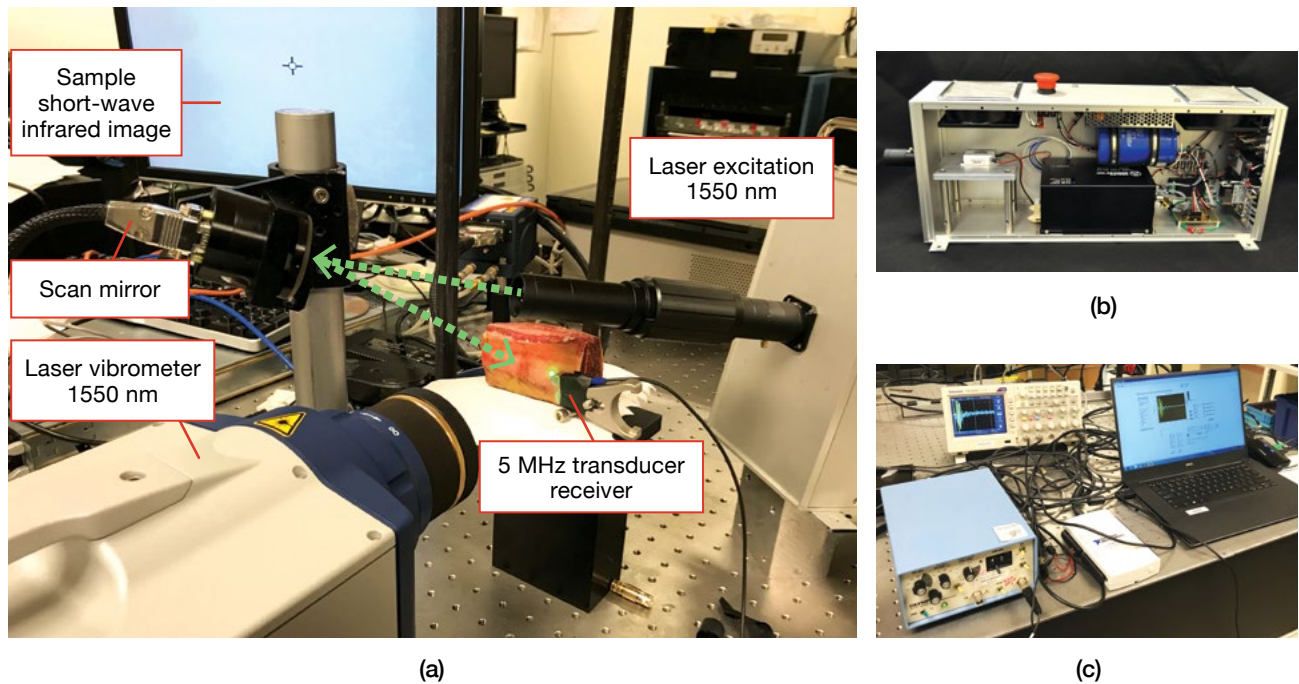
FIGURE 2. The N-CLUS proof-of-concept system (a) uses a customized photoacoustic source emitting a 1550-nanometer eye- and skin-safe pulse for excitation and a commercial laser Doppler vibrometer (LDV) to measure the returning ultrasonic wave. The LDV receive system is a Polytec RSV-150. A fast steering mirror scans and positions the optical beams on the biological tissue sample. The custom-built Lincoln Laboratory 1550-nanometer Q-switched pulsed laser (b) induces the photoacoustic effect to send an ultrasonic wave into tissue. The laser has a pulse repetition frequency (PRF) of 10 hertz and 1 millijoule of power per pulse. The N-CLUS approach's data acquisition system (c) comprises a Tektronix scope and a laptop. The mirror assembly can be controlled with LabView software to scan and position the excitation laser beam onto a tissue sample.

N-CLUS Eye- and Skin-Safe Operation and Performance

Critical factors to consider when one is designing an operational system for use by physicians are patient safety and risks related to system hazards; image quality; effective aerial coverage rates; size, weight, and power; and cost. We first evaluated the effects of an imaging system's optical excitation wavelength on the SNR, image quality, and skin and eye safety. To start, we examined the image quality produced by four different common optical excitation wavelengths that span the near- to short-wave infrared—810 nanometers, 1064 nanometers, 1550 nanometers, and 2000 nanometers—using the optical parametric oscillator at Lincoln Laboratory. For each of these wavelengths, a pulse with a 7-nanosecond rise time (the time it takes for a pulse to rise from its lowest value to its highest value) was transmitted; the fluence level of the laser beam on the sample's surface was held constant at 21 millijoules/square centimeter

(mJ/cm^2), and the laser spot on the sample's surface was 2 millimeters in diameter. To obtain the measurements, we used a beef steak sample that contained two 1-millimeter-diameter rods that were inserted lengthwise into the sample. The pulsed laser beam that launches the ultrasonic wave was scanned across the sample, and the LDV measured the returning waves from a location at the far end of the scan line. The data collected from this demonstration were then displayed to show a 2D cross section of a time series where the y-axis showed the two-way travel time of the ultrasonic wave and the x-axis showed the scan position of the excitation laser where the ultrasonic wave was launched.

In Figure 3b, the measured ultrasonic time-domain reflection data are compared in sonograms. As the optical wavelength increased, the observed ultrasonic frequency band also shifted higher relative to the optical absorption. Correspondingly, the sonograms showed ultrasonic reflection events sharpening with increasing

optical wavelength excitation. The ultrasonic amplitudes increased with increasing optical wavelengths up to the 1550-nanometer source, then showed a relative decrease for the 2000-nanometer source. Although the ultrasonic frequency content generated by the 2000-nanometer source is high and the associated image exhibits the best temporal resolution, the signal amplitude drops. This drop is likely caused by increased ultrasonic wave attenuation acting more severely on higher-frequency components as the ultrasonic wave traveled through the beef sample.

(a)
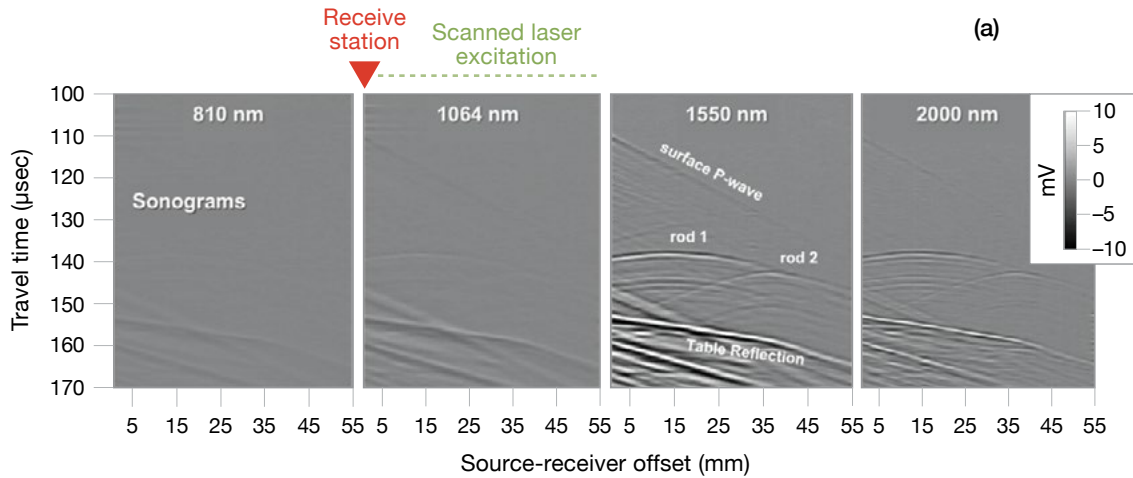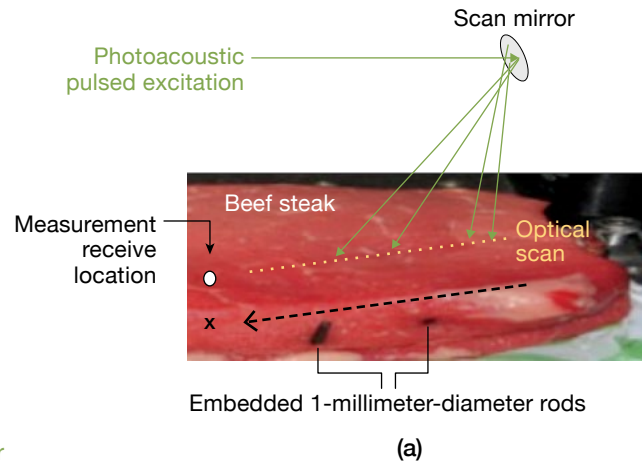
(b)
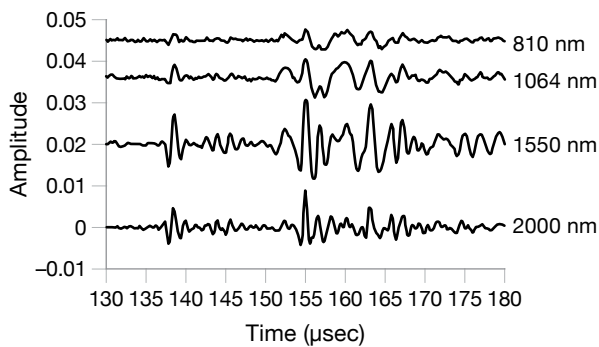
(c)
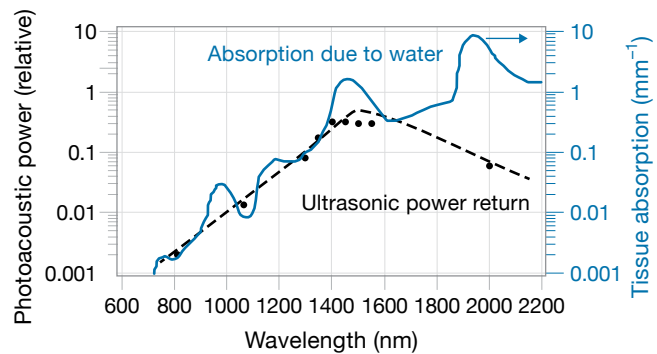
(d)

FIGURE 3. A beef steak sample is shown with the noncontact laser ultrasound geometry layout (a). Two 1-millimeter-diameter rods were embedded in the sample, and the pulsed laser was scanned across the sample by using a steering mirror. The scan line in this geometry is referred to as an off-end sonogram, where the receiver station is at the near end of the cross section, and the laser ultrasound excitation source is moved incrementally away from the receiver in a bistatic geometry. Noncontact laser ultrasound sonograms were produced for four stimulus wavelengths with a constant spot size and power per area (b). The 1550-nanometer source displayed the best image resolution. Also shown is a comparison of ultrasonic time-series traces for measurements directly over a 1-millimeter rod at four optical wavelengths (c). The 1550-nanometer and 2000-nanometer sources registered the rod the most clearly, as indicated by the amplitude level. On the bottom right, the chart shows the summed ultrasonic power of measured ultrasound returns as a function of optical excitation wavelength, and the optical absorption caused by water (the dominant material in biological tissue) as a function of optical wavelength (d).

ROBERT W. HAUPT, CHARLES M. WYNN, MATTHEW R. JOHNSON, JONATHAN R. FINCKE, XIANG ZHANG, BRIAN W. ANTHONY, AND ANTHONY E. SAMIR

Table 2 states the American National Standards Institute (ANSI)'s laser exposure limits for eye and skin safety for the four wavelength examples shown in Figure 3b [18]. The 1550-nanometer and 2000-nanometer sources produced images with the best SNR. The images showed the features of the metal rods, steak, and table top while maintaining optical excitation within skin- and eye-safety limits. The 810-nanometer and 1064-nanometer sources produced weaker SNR images for optical excitation fluence levels above the ANSI eye-safety threshold. The high optical absorptivity of the 1550-nanometer wavelength provides the highest eye-safety threshold, allowing high optical powers that improve the SNR while still maintaining safety. The 1550-nanometer source also offers common commercially ready components. Of the four wavelengths examined, the 1550-nanometer and 2000-nanometer sources provide the highest ultrasound image quality and SNR while providing the highest margin for safety.

N-CLUS Imaging in Biological Tissue

We next examine N-CLUS's ability to generate ultrasonic images using skin-and eye-safe laser powers in biological tissue and compare the system's performance to that of contact transducers and a GE 9-megahertz medical ultrasound probe. First, we scanned grocery store beef steak and pork samples with the N-CLUS 1550-nanometer photoacoustic source and used the Polytec RSV-150 vibrometer to measure the returning ultrasonic waves at the surface of each sample. We then used the N-CLUS system to generate anatomical images of tissue and bone in the forearm of a human test subject. To simulate more realistic patient conditions, particular attention was given to these measurements to ensure that the emitted optical powers were within skin- and eye-safety requirements.

Comparison of Medical Transducer Signal Quality to N-CLUS Signal Quality

If the N-CLUS approach is to lead to a viable medical system, it must produce high-quality interior images of tissue that are comparable to images acquired with conventional medical ultrasound. We first compare the signal with noise of N-CLUS to that of medical transducer technologies, which are shown in Figures 4 and 5. For the demonstration shown in Figure 4, we constructed

Table 2. ANSI Z136.1-2007 Skin and Eye Safety Optical Exposure Levels

WAVELENGTH (nm)	SKIN SAFETY THRESHOLD (mJ/cm^2)	EYE SAFETY THRESHOLD (mJ/cm^2)
810	33	8.3×10^{-4}
1064	105	5.0×10^{-3}
1550	1000	1000
2000	100	100

a simulated tissue sample with a PVC pipe embedded in a copolymer soft tissue material that had the same mechanical properties as human tissue. Compared methodologies included an all-acoustic transducer transmit and transducer receive system in a water tank [19]; a hybrid-acoustic optical photoacoustic transmit with acoustic contact transducer receive system; and an all-optical, totally noncontact laser ultrasound transmit-and-receive system.

In the water tank, the simulated tissue's surface was at a distance of 4 centimeters from the all-acoustic transmit-and-receive transducer configuration. The transducers were immersed in water to mitigate the effects of varying transducer application pressures and look angles. The three configurations depicted in Figure 4 show the signal-with-noise characteristics of each method for acquiring ultrasound data. All of the techniques show similar SNR for their time-series trace measurements of the returning ultrasonic signal. The traces shown for the all-acoustic (immersed in water tank) and the hybrid-acoustic (optical photoacoustic source using the contact transducer attached to the simulated tissue) methods exhibited the same approximate SNR for a single transmitted pulse response. This result indicates that the optical photoacoustic source is significantly efficient and is able to achieve an SNR that is reasonably comparable to that of the conventional all-acoustic transducer system. We conclude from this example study that the photoacoustic source used at 1550 nanometers is potentially competitive, in terms of efficiency and quality, with a single medical ultrasound transducer.

In the third plot in Figure 4, the N-CLUS-acquired trace is shown in comparison to the results of the other

two methods. The laser vibrometer's measurement was averaged over 128 repeated pulse response collections to improve the SNR. The vibrometer performance is driven by its shot noise and speckle noise. To be competitive with conventional all-acoustic transducer systems, the laser-sensing capability of N-CLUS requires significant averaging.

Note that only the all-acoustic transducer approach used the water tank, which required transducers to be submerged. Optical methods are immersion free, require a line of sight in the air, and can be steered by a mirror.

Although all-acoustic water tank ultrasound can provide high-quality data and images, the water tank itself has serious drawbacks for field-forward applications because of its size, weight, and complexity. Furthermore, the water tank is often uncomfortable for patients to immerse their body parts in for measurement. It is highly impractical to immerse the entire torso, so measurements are limited to the extremities.

The measurements demonstrated in Figure 4 show that a photoacoustically generated ultrasonic wave in tissue can be comparable in magnitude and SNR to
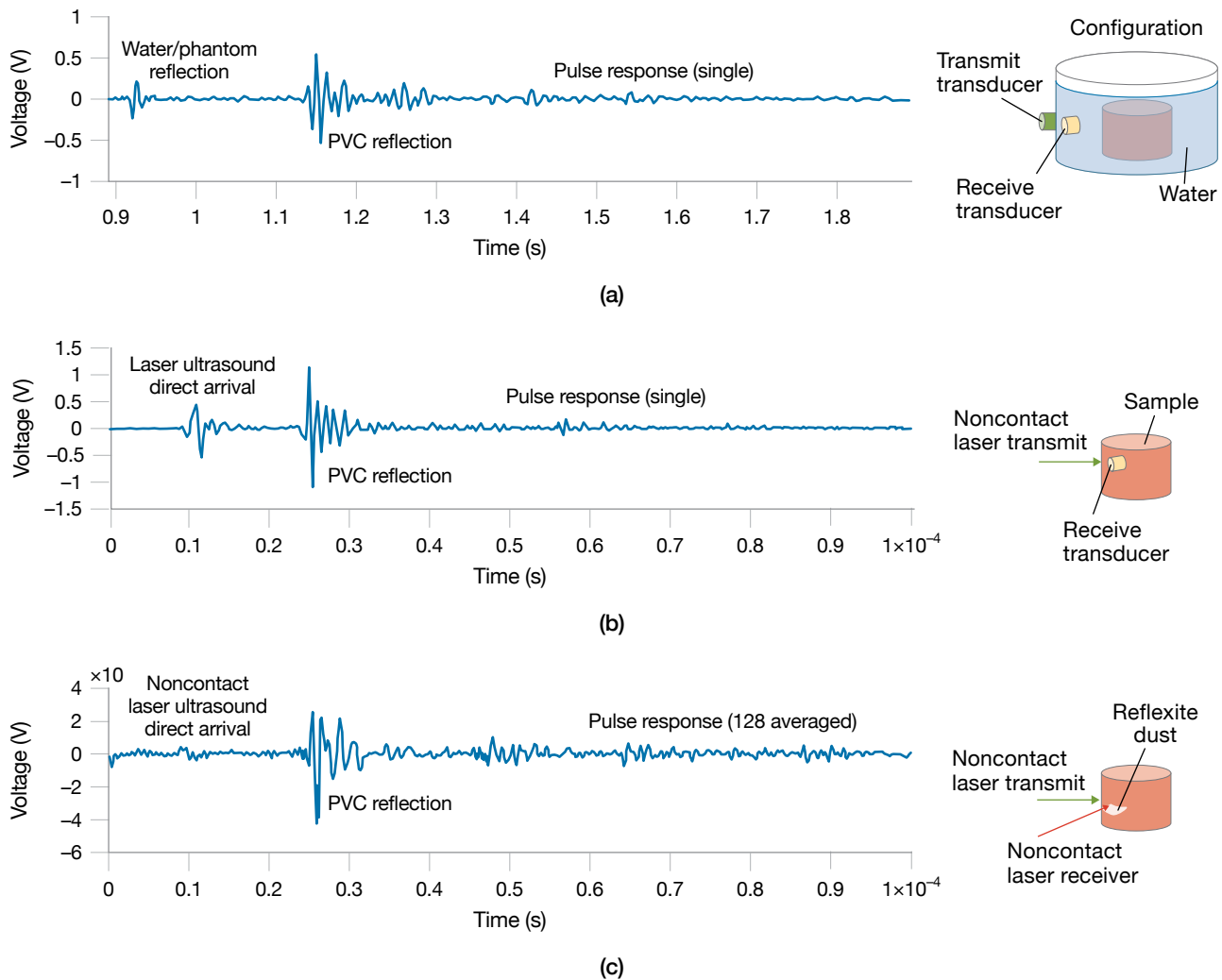
FIGURE 4. We compared time-series traces measured by state-of-the-art all-acoustic piezoelectric transducers submerged in a water tank (a), a hybrid-acoustic optical laser photoacoustic excitation measured by a contact Olympus V152 longitudinal wave 1-megahertz transducer (b), and an all-optical total noncontact laser ultrasound (c). The noncontact ultrasound's time-series trace closely resembles those of the ultrasound transducers, indicating that waves generated by the noncontact system are comparable in magnitude and SNR to waves generated by traditional transducers.

waves produced by medical ultrasound transducers. We next constructed 2D sonograms of a complex soft tissue mass containing bone to compare the skin- and eye-safe N-CLUS system to optically generated ultrasound (photoacoustic) that utilizes contact transducers (1-megahertz Olympus V152 longitudinal wave). In the demonstration shown in Figure 5, a 3-inch-thick beef steak sample containing a rib bone was scanned with the full N-CLUS system (10-hertz PRF, 1550-nanometer optical-to-ultrasound excitation, and 1550-nanometer Polytec laser vibrometer receiver) to produce an ultrasound image. The full N-CLUS image was compared with the image produced by a hybrid acquisition method that paired photoacoustic excitation with a contact ultrasound transducer. Each time-series trace used in each image had a listen time of 200 microseconds, which provided enough time to capture the ultrasonic signals-of-interest returns from the steak sample. The laser vibrometer and transducer were filtered to a bandwidth of 1.5 megahertz for comparison. The beef sample had no optical treatment to enhance the laser vibrometer's performance. A water-based medical gel was used to enhance coupling of the transducer to the beef sample's surface (using gel is a standard medical practice in ultrasound). The emitted optical beams were within skin- and eye-safety limits.

The geometry of the beef sample's internal features are well captured in both images. The fat layers and bone are clearly evident because the traveling ultrasonic wave encounters more resistance at these features, thus causing a strong acoustic impedance signature. We next compared ultrasound images acquired with the N-CLUS technique to images acquired with a state-of-the-art General Electric (GE) 9-megahertz medical ultrasound system, as shown in Figure 6. In this example, the photoacoustic source and LDV beams were collocated and scanned across the sample.

In both the N-CLUS and GE Array images, the fat layer geometries are clearly evident. However, the spatial resolution is significantly better for the ground truth GE system's image. The lower resolution of the N-CLUS image is primarily because the set bandwidth of the receiving laser vibrometer is limited at 1 megahertz. The GE system also employs array-processing methods to further improve the spatial resolution. It is anticipated that increasing the laser vibrometer bandwidth
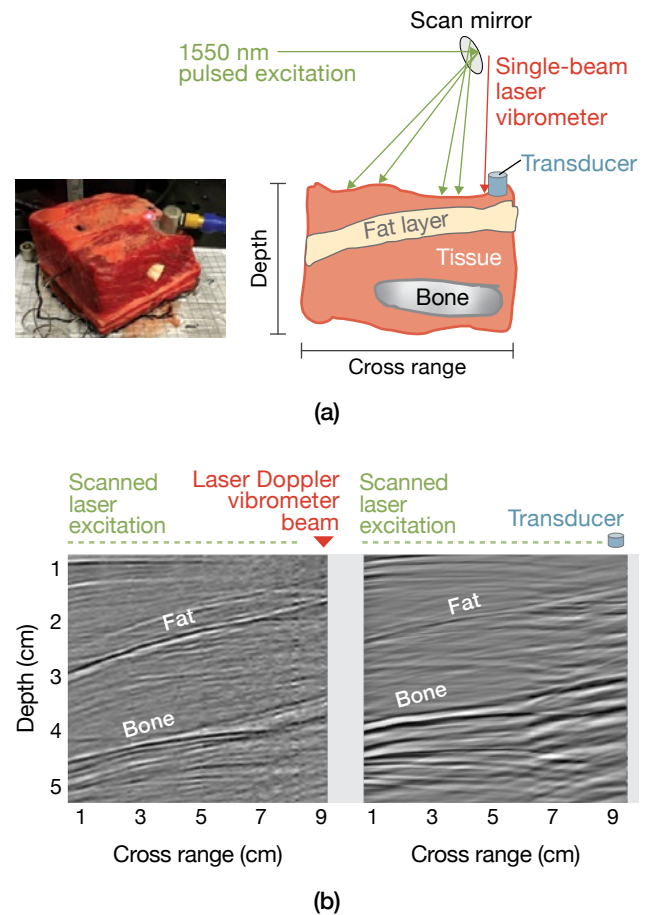
(a)

(b)

FIGURE 5. A 3-inch-thick beef steak sample containing a rib bone was scanned with the full N-CLUS system (photoacoustic source with stationary LDV receiver) and then with a hybrid system that paired a photoacoustic source with an Olympus V152 longitudinal wave 1-megahertz transducer (a). The transducer and LDV were approximately collocated. The sonograms produced by both systems are shown converted to depth (b). Both the total N-CLUS system (left) and the scanned photoacoustic source with the transducer (right) clearly displayed the fat and bone features within the steak sample.

by a factor of nine would improve the N-CLUS system's image resolution and bring it closer to the resolution of the GE system.

At present, the N-CLUS system is much slower than the commercial GE system in terms of data acquisition. The largest factor impeding the N-CLUS data acquisition rate is the very slow 10-hertz PRF of the 1550-nanometer optical excitation laser that generates the ultrasonic pulse. In Figure 6, 100 excitation positions constituted the data acquisition scan, and the scan required 10 seconds for each pulse excitation. The total time was increased even
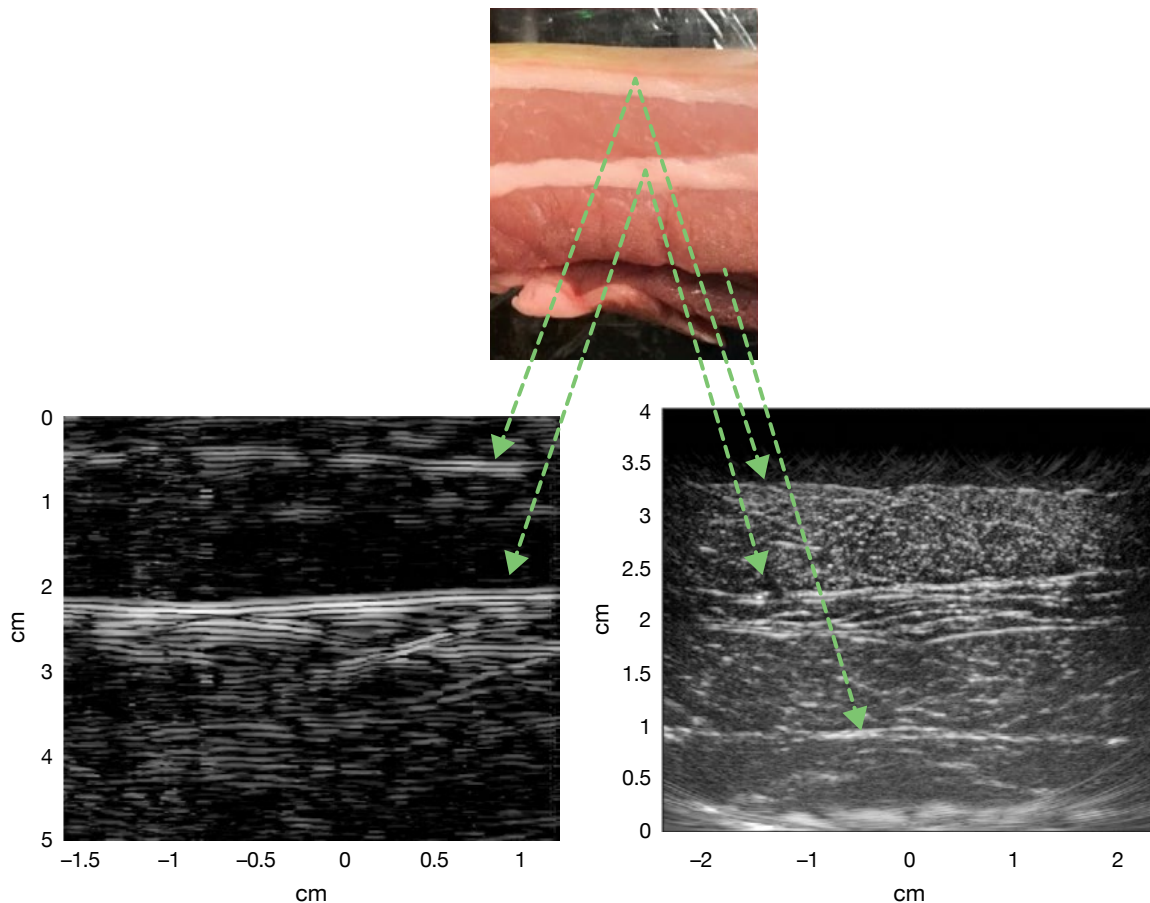
FIGURE 6. The above figure shows the N-CLUS sonograms of a scanned pork sample, converted to depth. Comparisons are shown for the total N-CLUS system (collocated scanned photoacoustic source and scanned laser Doppler vibrometry beam) (left) and the GE 9-megahertz medical ultrasound system (right). The fat layers of the pork sample can be seen in the sonograms for both systems.

further because acquiring the N-CLUS image involved averaging 64 data-trace collections per scan location, and it took approximately 10 minutes to acquire the entire dataset. The laser vibrometer required averaging to yield a useful SNR for the returning signal.

N-CLUS Eye- and Skin-Safe Images of a Human Test Subject

By using the N-CLUS and GE 9-megahertz systems, we acquired 2D cross-sectional ultrasound images of a human test subject's forearm. For these image constructions, the N-CLUS optical excitation and laser vibrometer beams were slightly offset (about 0.5 centimeters apart) and then scanned together across the test subject's skin. The N-CLUS optical powers were consistently maintained to be skin and eye safe. No optical treatment was applied to the surface of the test subject's skin to enhance the

laser vibrometer's performance. However, for the GE 9-megahertz system demonstration, a water-based gel was applied to the subject's skin to enhance ultrasound coupling during operation of the GE 9-megahertz transducer head.

In both the N-CLUS and GE Array images, fat layers, a tendon, and bone features are clearly evident. However, the spatial resolution is again significantly better for the GE system's image. The N-CLUS image has a lower resolution because, as previously mentioned, the set bandwidth of the receiving laser vibrometer is limited at 1 megahertz. The N-CLUS system required less than five minutes to acquire the entire dataset in the examples shown in Figure 7.

Another important factor to consider when using the N-CLUS system to collect data is patient motion. It becomes increasingly difficult for a patient to remain

ROBERT W. HAUPT, CHARLES M. WYNN, MATTHEW R. JOHNSON, JONATHAN R. FINCKE, XIANG ZHANG, BRIAN W. ANTHONY, AND ANTHONY E. SAMIR

(a)

(b)

(c)

(d)
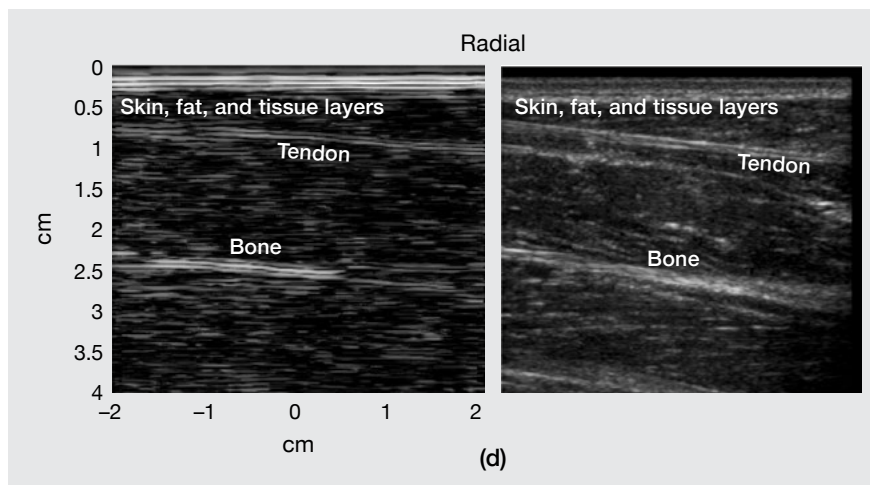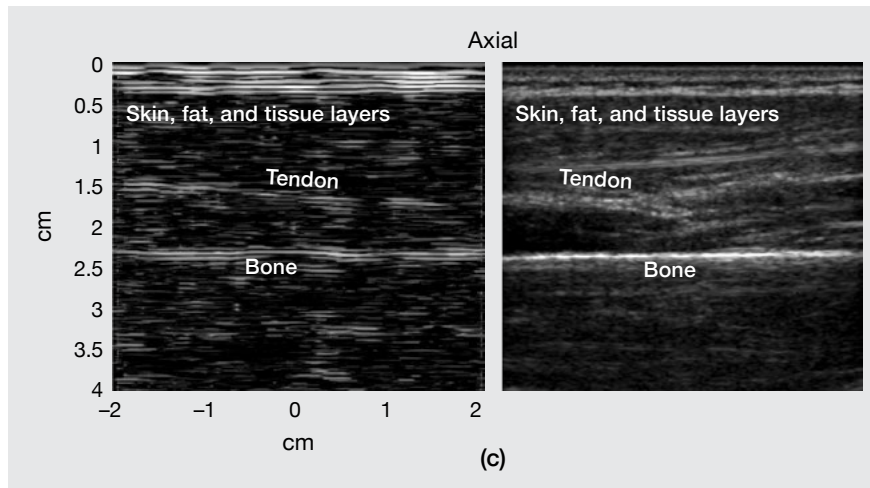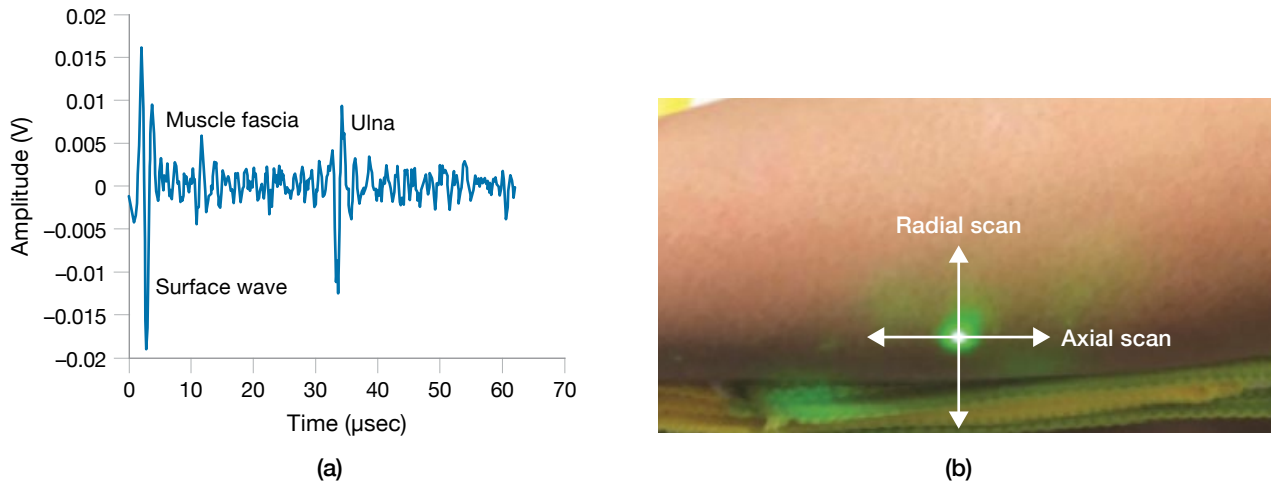
FIGURE 7. This graph shows the results of a time-series data measurement acquired with a laser Doppler vibrometer (a). The spikes in amplitude show the direct ultrasonic surface wave and the subsequent reflections off tissue and bone in the test subject's arm. The subject's arm was scanned in the radial and axial directions (b). The green spot is an eye- and skin-safe reference laser that marked the position of the infrared 1550-nanometer laser beam, which is not visible to the naked eye. The N-CLUS sonograms were converted to depth [27] for scans of the subject's forearm in the axial direction (c) and the radial direction (d). Comparisons are shown for the total N-CLUS system (collocated scanned photoacoustic source and scanned LDV beam) (left) and the GE 9-megahertz medical ultrasound system (right). Internal features of the arm, such as tissue layers, a tendon, and bone, can be seen in the sonograms for both systems.

motionless for periods longer than several seconds. Patient motion, such as sudden jerks or readjustment to become comfortable, results in partial shifts in the resulting image or static breaks causing misalignment between trace collections when they are averaged. To overcome the effects of patient motion on image quality, the N-CLUS system's data-acquisition time needs to be significantly shortened. Many patient-motion effects can be mitigated by using higher-PRF optical excitation systems. Optical short-pulse systems (5-nanosecond pulses operated at a

PRF of 5 kilohertz) that are available on the commercial market can also provide optical powers on the order of one to several millijoules per pulse. At the appropriate optical wavelength, these powers are skin and eye safe. The fast PRF can decrease the total time needed for data acquisition by a factor of 500. Applying a fast excitation PRF to the N-CLUS system reduced its data-acquisition time from 1 to 10 minutes to approximately 1 second. Because the time required to take a measurement is much shorter when a short PRF is applied, the effects of patient motion will be greatly reduced, enabling the N-CLUS scanning approach to be more feasible than before for operational and practical ultrasound.

The results discussed in this section are a first in the medical literature. We produced anatomical images by using skin- and eye-safe laser ultrasound within test tissue samples without using surface treatments to enhance the optical return for a laser vibrometer measurement. Moreover, this is a first in the medical literature in performing such measurements successfully on a human test subject and producing a useful anatomical image [20–24].

Use of N-CLUS for Elastography Measurements and Novel Applications

Elastography is an emerging field in medicine that noninvasively measures the mechanical properties and determines the spatial distribution of tissue, organs, and bones in a patient's body. Evaluation of elastographic properties entails quantifying the stiffness distribution of tissue. The degree of stiffness and compliance (the ability of an organ to increase its volume with pressure) indicates tissue type and health. For example, stiffening of liver tissue can imply fibrosis of the liver, which is a serious health condition. Elastography is increasingly being used for investigating disease conditions in internal organs. It can also be used as diagnostic information to supplement anatomical images. Elastography can be used to guide biopsies or to replace them entirely. Biopsies are invasive and painful and present a risk of hemorrhage or infection, whereas elastography is completely noninvasive. Elastography is now commonly used for the detection and diagnosis of breast, thyroid, and prostate cancers. Certain types of elastography are also suitable for musculoskeletal diagnosis and can determine the mechanical properties and states of muscles and tendons.

To produce anatomical images, we exploited far-field ultrasonic waves that reflect and transmit within soft tissue in the body's interior. We present a novel approach to acquiring the elastographic properties of bone with the N-CLUS system, which can reveal the elastic moduli by using far-offset surface waves that travel within the outer surface layers of bone. Far-offset surface waves in bone can be induced and measured by using a bistatic configuration in which the photoacoustic source and laser vibrometer receiver are widely separated. The diving wave travels along the tissue-bone interface and re-emerges at a long offset, as depicted in Figure 8a.

The surface longitudinal and shear wave events are exhibited simultaneously in the ultrasound sonogram for a bistatic long-offset measurement shown in Figure 8c. The wave speeds were determined from the slope of each wave event. The shallow slope, or the faster wave, is that of the longitudinal wave (V_p), and the steeper slope is that of the shear wave (V_s). Once these speeds were determined, the elastic moduli were computed from the expressions shown in Figure 8 [25].

The results shown in Figures 7 and 8 are a first in the medical literature. We produced elastographic and measurements of bone defects by using skin- and eye-safe laser ultrasound on test tissue samples and without a surface treatment to enhance the optical return for a laser vibrometer measurement. In addition, it is likely a first that we were able to show that shear wave events in bone can be measured with a totally noncontact laser method.

Novel N-CLUS Applications

The N-CLUS concept was initiated and formulated for multiple medical applications that utilize anatomical imaging and elastographic capabilities separately or combined. There are currently no optoacoustic systems for medical applications in existence or in near-term development. The ability to perform contact-free ultrasound scans could improve the image quality and portability of ultrasound tomographic devices and could expand ultrasound applications. The main benefit of N-CLUS is that the noncontact optical approach attempts to minimize operator variability. Such an approach is envisioned to allow repeat-visit ultrasound measurements that can be compared to each other with enough accuracy to enable change detection. Recent work by other groups has focused on using fixed-frame water tank/gel bath

ROBERT W. HAUPT, CHARLES M. WYNN, MATTHEW R. JOHNSON, JONATHAN R. FINCKE, XIANG ZHANG, BRIAN W. ANTHONY, AND ANTHONY E. SAMIR

(a)

(b)

IN VIVO ELASTIC MODULI DETERMINED FROM ULTRASONIC VELOCITIES

YOUNG'S MODULUS	POISSON'S RATIO	BULK MODULUS	SHEAR MODULUS
$\rho V_{\mathrm{s}}^2 \left(3V_{\mathrm{P}}^2 - 2V_{\mathrm{s}}^2 \right)$ $/ \left(V_{\mathrm{P}}^2 - V_{\mathrm{s}}^2 / 3 \right)$	$\left(V_{\mathrm{P}}^2 - 2V_{\mathrm{s}}^2 \right)$ $/ 2 \left(V_{\mathrm{P}}^2 - V_{\mathrm{s}}^2 \right)$	$\rho \left(V_{\mathrm{P}}^2 - 4V_{\mathrm{s}}^2 / 3 \right)$	ρV_{s}^2
21.0 GPa	0.3474	22.5 GPa	7.6 GPa

where

　Longitudinal (V_{P}) is 3890 m/s

　Rayleigh (V_{s}) is 1711 m/s

　Shear is Rayleigh / 0.91 = 1881 m/s

(c)

FIGURE 8. The N-CLUS system can be used to determine a bone sample's elastographic properties by using a far-offset receiver and source geometry to induce an ultrasonic surface wave in the bone (a). The wave traveled along the outer layers of the bone and returned to the surface, where it was measured by the laser Doppler vibrometer (b). The surface longitudinal and shear waves measured by N-CLUS are shown in the ultrasound sonogram created from this demonstration (c). The shear wave speed, compressional wave speed, and bone density are represented by V_{s}, V_{P}, and ρ, respectively. The wave speeds were calculated from the slope of each wave, and the elastic moduli were determined by plugging the wave speeds into mathematical equations (c).

approaches for performing change-detection ultrasound, such as tomography for cancer screening. While the images obtained with these systems have resolutions comparable to those of images obtained with MRI, these systems are generally designed exclusively for breast imaging, are unlikely to become portable, and cannot detect high-frequency shear waves (because the transducers are housed in water, shear attenuates drastically over submillimeter distances).

Applying ultrasound techniques to soft tissue containing bone presents additional imaging challenges. The strong refraction, attenuation, and scattering of transmitted acoustic waves used for imaging must be overcome. The ability to measure all waves (longitudinal,

shear, etc.) at many locations by using noncontact optoacoustic techniques promises to aid in meeting these challenges. Thus, a noncontact optoacoustic system capable of accurate characterization of bone and the surrounding soft tissue has the potential for unique applications, several of which we have explored: (1) improving prosthetic fittings by integrating internal tissue and bone structural information into the socket design process; (2) monitoring bone-density deterioration related to osteoporosis; (3) scanning load-bearing bones for stress fractures and early stages of damage; and (4) better quantifying the progression of neuromuscular disease.

N-CLUS Approach for the Detection and Imaging of Bone Injuries

The N-CLUS has the potential to detect and monitor common and debilitating bone injuries, such as stress fractures. When the bistatic far-offset acquisition geometry is utilized, N-CLUS generates refracted surface waves that produce the acoustic signatures of simulated bone defects that are similar in scale to stress fractures. In the demonstration shown in Figure 9, we introduced a 1-millimeter-deep by 1-millimeter-wide drill hole in the surface of a rib bone embedded in beef tissue. The beef tissue lying over the bone was approximately 2 to 4 millimeters thick. Once the small drill hole was made, the beef tissue was repositioned over the drill hole to maintain tissue continuity as would be expected in an actual tissue-bone setting.

Several scan lines were collected along the length of the bone. As observed in Figures 9b and 9c, refracted surface longitudinal and shear wave events dominate the sonogram. The green circled area shows the acoustic interference signature from these waves. It is important to note that though the simulated defect may be similar in scale to a common stress fracture, the material property contrasts may be more subtle in an actual stress fracture and result in a less pronounced signature, if any. Nonetheless, this example shows there may be potential in using the N-CLUS approach to detect, image, and monitor bone injuries such as stress fractures.

Prosthetic Fitting Using N-CLUS

We next show the potential of N-CLUS to acquire images of large-scale bone surrounded by soft tissue for applications in elastography, prosthetic limb fitting,

and prosthetic socket design. We employed a simulated residual limb (called a phantom model) containing a bone/muscle complex to demonstrate how N-CLUS's reflection and tomographic imaging capabilities could be used to optimize prosthetic fitting for an amputated limb.

The phantom limb shown in this example was constructed from a PVC pipe segment embedded in a copolymer soft tissue material. To reconstruct an image by using N-CLUS, one must know the target object's geometry, its surface topography, and the receiver and source locations. To obtain the topography, a NextEngine 3D laser scanned the phantom's surface and output the phantom's geometry in a 3D point cloud. A reference mark on the phantom allowed alignment between the laser source and receiver to the 3D-scan reference frame. Once the 3D scan was completed, the phantom was placed on a Sigma-Koki SGSP-YAW rotation stage with a 0.005-degree angular resolution. The N-CLUS source was driven by an optical parametric oscillator Q-switched laser with a fixed wavelength of 1550 nanometers, a 3-nanosecond pulse width, and a 3-millimeter projected spot diameter on the phantom. A Polytec OFV 505 laser vibrometer was used to measure the induced ultrasonic returns at a fixed location on the phantom's surface.

The data-acquisition process consisted of sending a laser pulse that excited a photoacoustic converted ultrasonic wave at the phantom's surface and receiving the return propagating wave with the laser vibrometer. For each transmit-and-receive location, the signal was averaged 64 times to obtain the SNR needed to create reasonable images and estimate travel times. Next, the stage rotated by two degrees, and the pulse-receive process was repeated until the stage completed a full 360-degree revolution. Once a full revolution was completed, the laser vibrometer's position was moved 30 degrees, and the pulse receiving process was repeated again. The data acquired during one full revolution of the rotation stage are equivalent to the data acquired by transmitting on one element and receiving on all others for a 180-element circular array fixed to the phantom's surface. In total, the dataset is analogous to sequentially transmitting on 12 elements each spaced by 30 degrees and receiving on all other elements for each transmit.

Standard migration routines produced the pulse echo image in Figure 10c, and the blockwise inversion technique [19] produced the sound-speed map in Figure 10d. One

ROBERT W. HAUPT, CHARLES M. WYNN, MATTHEW R. JOHNSON, JONATHAN R. FINCKE, XIANG ZHANG, BRIAN W. ANTHONY, AND ANTHONY E. SAMIR
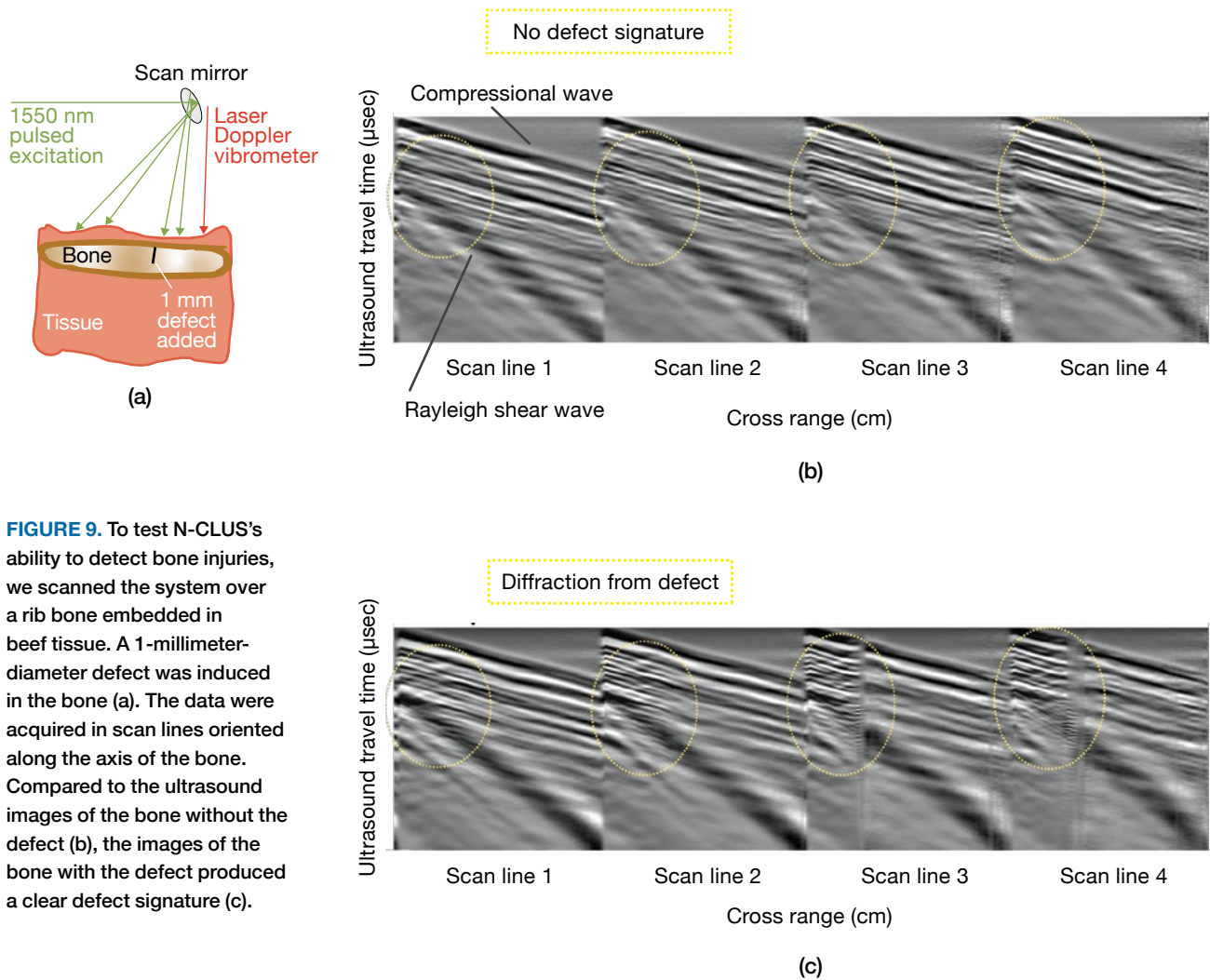
FIGURE 9. To test N-CLUS's ability to detect bone injuries, we scanned the system over a rib bone embedded in beef tissue. A 1-millimeter-diameter defect was induced in the bone (a). The data were acquired in scan lines oriented along the axis of the bone. Compared to the ultrasound images of the bone without the defect (b), the images of the bone with the defect produced a clear defect signature (c).

of the critical issues with reconstructing images from laser ultrasound data is localizing the transmitter and receiver locations on the target. In this case, the use of a 3D scan and a rotational stage with a stationary target provided known measurement positions in a precise way, allowing the use of standard ultrasound reconstruction algorithms. The pulse echo image showed the diameter of the pipe to be 0.035 meters, and the true radius was 0.0334 meters. The estimate of the limb's sound speed was 1396 meters/second, and the estimate of the pipe's sound speed was 1934 meters/second. The true sound speed was 1406 meters/second for the limb and 2100 meters/second for the PVC pipe. As evidenced by the results, the system is able to quantify a tissue-like target with accuracy on the order of a few acoustic wavelengths.

Developing N-CLUS for Practical Medical Use

The demonstration system shown in Figure 2 asserts that N-CLUS can produce anatomical images and elastographic data for several applications. However, the N-CLUS system in its present form is not sufficiently operational for clinical use. Significant improvements need to be developed that would enable N-CLUS to provide images and data that are comparable and competitive with those of current state-of-the-art ultrasound systems used in medical practice. However, new components on the market now can enable a rack-mounted system that may be fast enough and sensitive enough to be used in a clinical or remote field-forward station in the very near term.

High-PRF Photoacoustic Source

High-power, high-PRF pulsed lasers that can produce photoacoustic ultrasound while operating within skin- and eye-safety limits have recently become available on the commercial market. We observed that a single optical pulse with a power of 1 millijoule and 1- to 10-nanosecond duration can easily generate a strong ultrasonic wave in tissue in the desired acoustic band of a few megahertz. These optical sources now can operate at a PRF of 5 kilohertz and provide continuous time coverage when the system listens for signals comprising an individual time-series trace of 200 microseconds. Current pulsed optical systems have been reduced in size and can be rack mounted. Private companies are
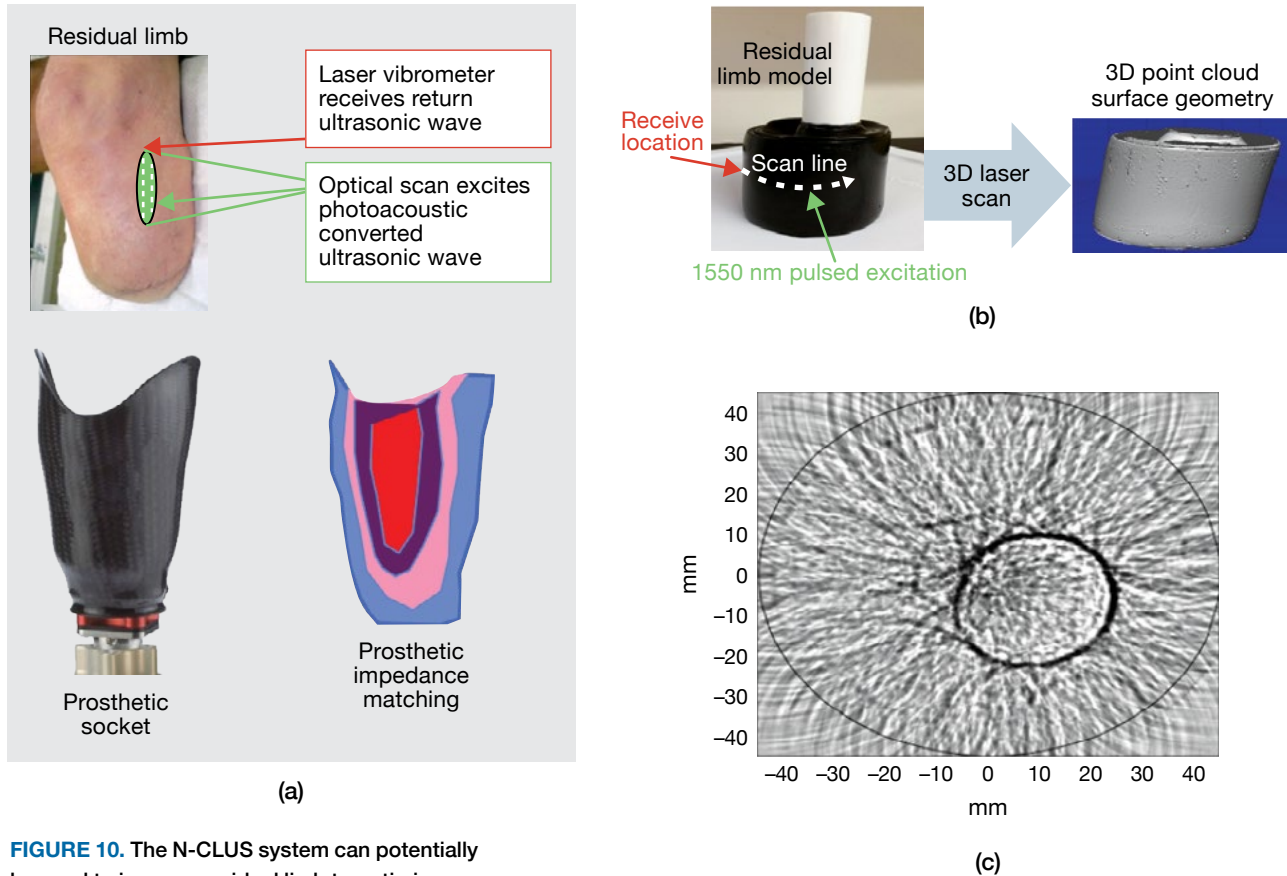
FIGURE 10. The N-CLUS system can potentially be used to image a residual limb to optimize prosthetic fitting for amputees (a). We constructed a simulated residual limb (phantom) out of a PVC pipe surrounded by a soft tissue–like material (b). The phantom was first scanned by a 3D laser and then placed on a rotating platform before it was scanned by the N-CLUS system, which was held at a constant location. A pulse echo image (c) and a sound speed map (d) of the phantom were produced from the scans. In the pulse echo image, the PVC pipe (which simulates bone) was distinct from the surrounding soft tissue material. The speed of the ultrasonic wave traveling in the soft tissue material and in the PVC pipe was determined from the N-CLUS measurements. These speeds closely matched the same wave speeds that were determined from measurements produced by contact transducers.

pushing to miniaturize these sources, and handheld, high-power, high-PRF systems are anticipated to be available in a year or two. The improved PRF can decrease N-CLUS's image data-acquisition time from 10 minutes to around 1 second. To accomplish the high PRF while maintaining skin and eye safety, we constructed a 1950-nanometer-wavelength Q-switched laser that generates optical 2-millijoule, 5-nanosecond pulses and 1000 to 5000 of these pulses per second. A simple fast scanning mirror can be used to steer the optical excitation beam on the skin's surface.

Multipixel Laser Vibrometer

In our studies, the N-CLUS demonstration system's single-pixel laser vibrometer operating at 1550-nanometer and 10-milliwatt power (skin and eye safe) was able to measure returning ultrasonic signals. However, variations in optical speckle and in the surface diffusion of tissue caused significant subsecond time-scale fluctuations in the noise floor and in the performance of the laser vibrometer. To overcome these fluctuations, the laser measurement required averaging consecutive time-series traces at a given location to reduce the noise variance enough that the ultrasonic signal of interest could be observed above the noise floor. The acquisition time was increased even further because producing the N-CLUS image involved averaging 64 data trace collections per scan position location.

To implement a laser vibrometer ultrasound receiver that can meet the area coverage rate requirements in a clinical setting, a multipixel laser vibrometer system will be necessary. The multipixel configuration should be designed to capture multiple speckle lobes in the receive laser beam simultaneously for a given station position. Statistically, some of the speckle lobes will capture small noise contributions, while other lobes will capture large contributions. The pixels associated with large noise can be excluded, while pixels with small noise will be kept and averaged to reduce the noise variance further.

Currently, commercial vendors have been developing multipixel vibrometer systems that can measure ultrasonic vibrations on surfaces. These systems, which we have incorporated into the N-CLUS receiver design, can be readily adapted to use skin- and eye-safe optical wavelengths and powers for medical ultrasound imaging systems. To accomplish simultaneous averaging, we constructed a 48-pixel skin- and eye-safe LDV, pictured in Figure 11. This vibrometer measures several speckle lobes of the vibrational ultrasound signal simultaneously, and we keep the strong SNR returns, discard the weak returns, and average.
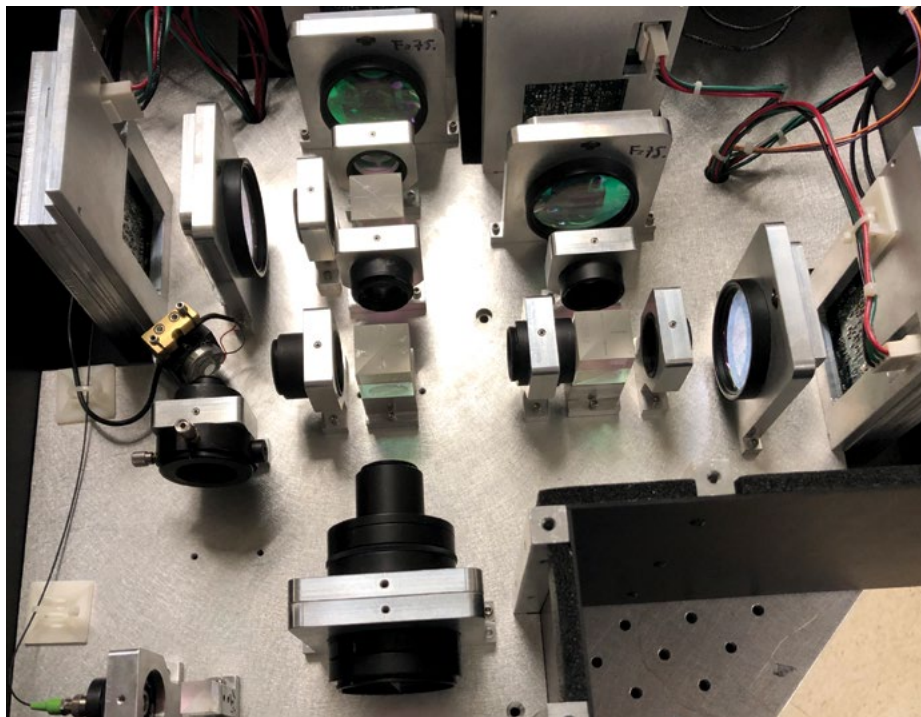
FIGURE 11. The skin- and eye-safe laser Doppler vibrometer utilizes 48 pixels simultaneously. The system has a bandwidth of 5 megahertz and uses 2-inch collection optics that can be operated from a standoff distance of 100 to 500 millimeters. The laser has an output of 10 milliwatts and an adjustable manual focus.

Stand-Mounted and Handheld N-CLUS System

Results from our studies show that a rack-mounted optoacoustic system for medical imaging could be assembled in the near term. As demonstrated in Figure 12, the optical head would be small enough to mount on a stand, and the head could be positioned over the target area on the patient's body and then scanned to acquire ultrasound data. Such a system could be used in a clinical setting or remote field-forward station. A high-PRF photoacoustic source and multipixel laser vibrometer can be implemented in the system.

In the long term, there is a significant desire to develop a small, portable, handheld noncontact optoacoustic system such as the one envisioned in Figure 13. Such a system will require miniaturization of components and will also require methods to compensate for operator motion and look angles, as is necessary for conventional handheld contact ultrasound systems. The use of chip-scale lidar technology is proposed to enable miniaturization and compensate for motion. Large numbers of pixels are being proposed to meet operational coverage rates required for full-body-scan ultrasound. At Lincoln Laboratory, we are investigating the components
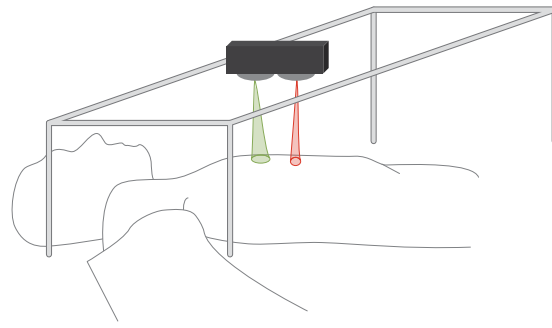
FIGURE 12. A simple stand mount for acquiring static N-CLUS measurements is proposed. The optical head is fixed in the stand and can be positioned anywhere in the frame by using a joy stick. Optical excitation and measurement laser beams can be scanned over a region of the body by using fast scanning mirrors. The electronics associated with the optical head can be rack mounted. The system would be portable enough to be assembled and used in a clinical setting or in a remote field-forward station.

needed for this capability. Technology such as Lincoln Laboratory–developed coherent focal plane arrays are being considered as a solution to handle the high data rates and coverage of medical ultrasound at frequency bandwidths of several megahertz. ∎
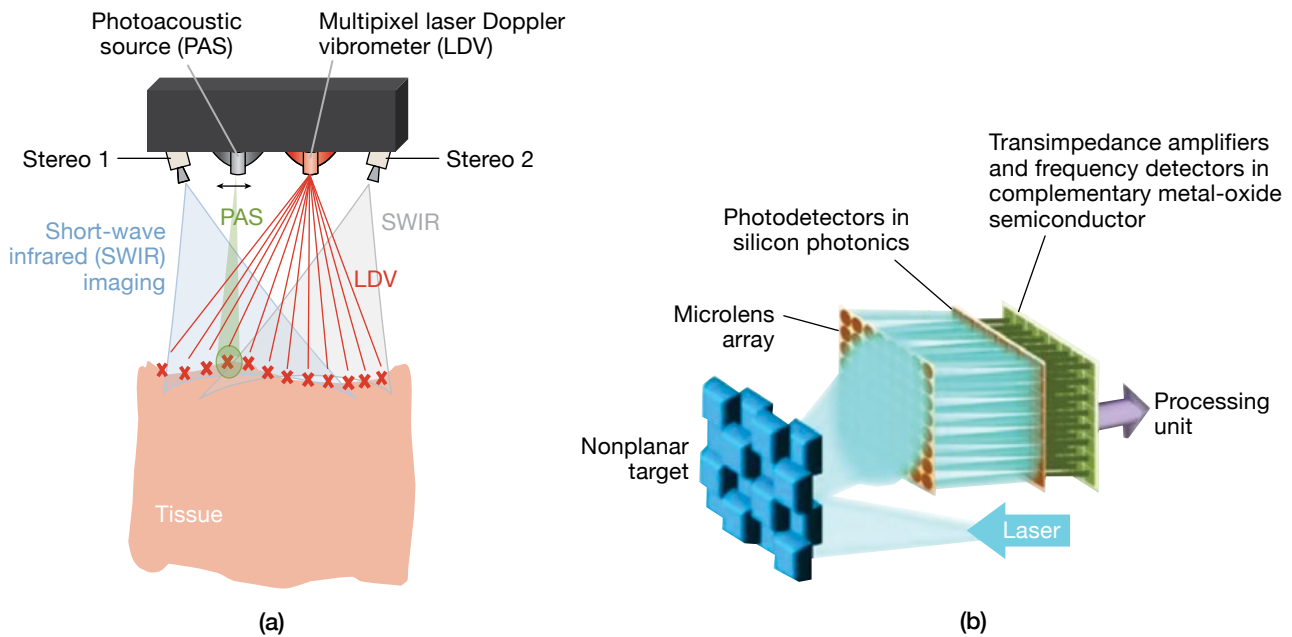
FIGURE 13. A portable handheld N-CLUS system concept is illustrated (a). The system would contain a photoacoustic source and a laser Doppler vibrometer on the same unit. Coherent focal plane arrays (b) are being considered as an element to integrate into medical ultrasound, but significant development is needed to implement chip-scale lidar and coherent focal plane array technology on medical devices.

ROBERT W. HAUPT, CHARLES M. WYNN, MATTHEW R. JOHNSON, JONATHAN R. FINCKE, XIANG ZHANG, BRIAN W. ANTHONY, AND ANTHONY E. SAMIR

References

1. W. Hendee and E. Ritenour, *Medical Imaging Physics*. New York: Wiley-Liss, 2002.

2. American Thyroid Association, "American Thyroid Association Guidelines," 2015, available at https://www.thyroid.org/professionals/ata-professional-guidelines/.

3. E.A. Eisenhauer, P. Therasse, J. Bogaerts, L.H. Schwartz, D. Sargent, R. Ford, et al., "New Response Evaluation Criteria in Solid Tumors: Revised RECIST Guideline (Version 1.1)," *European Journal of Cancer*, vol. 45, no. 2, 2009, pp. 228–247.

4. R.W. Haupt, C.M. Wynn, K. Holman, J. Kyung, and A. Samir, "Noncontact Laser Ultrasound (NCLUS)—Method to Mitigate Operator and Inter-operator Variability," U.S. patent application no. 62/309497, applied 17 Mar. 2016.

5. C.A. Pulafito, R. Birngruber, T.F. Deutsch, J.G. Fujimoto, D. Stern, and B. Zysset, "Laser-Tissue Interactions in the Nanosecond, Picosecond, and Femotosecond Time Domains," *Photoacoustics and Photothermal Phenomen II—Springer Series in Optical Sciences*, vol. 62, 1990, pp. 420–427.

6. L.V. Wang, "Tutorial on Photoacoustic Microscopy and Computed Tomography," *IEEE Journal of Selected Topics in Quantum Electronics*, vol. 14, no. 1, 2008, pp. 171–179.

7. M. Xu and L. Wang, "Photoacoustic Imaging in Biomedicine," *Review of Scientific Instruments*, vol. 77, no. 4, 2006.

8. C. Li and L.V. Wang, "Photoacoustic Tomography and Sensing in Biomedicine," *Physics in Medicine and Biology*, vol. 54, no. 19, 2009, pp. R59–R97.

9. B. Yin, D. Xing, Y. Wang, Y. Zeng, Y. Tan, and Q. Chen, "Fast Photoacoustic Imaging System Based on 320-Element Linear Transducer Array," *Physics in Medicine and Biology*, vol. 49, no. 7, 2004, pp. 1339–1346.

10. G. Xu, C. Wang, T. Feng, D. Oliver, and X. Wang, "Noncontact Photoacoustic Tomography with a Laser Doppler Vibrometer," *Proceedings of the Society of Photo-optical Instrumentation Engineers (SPIE)*, vol. 8943, 2014.

11. G. Rousseau, A. Blouin, and J. Monchalin, "Noncontact Photoacoustic Tomography and Ultrasonography for Tissue Imaging," *Biomedical Optics Express*, vol. 3, no. 1, 2012, pp. 16–25.

12. R.W. Haupt and C.M. Wynn, "System and Method for Noncontact Ultrasound," U.S. patent application no. 14/538698, issued 15 Jun. 2019.

13. A.R. Fisher, A.J. Schissler, and J.C. Schotland, "Photoacoustic Effect for Multiply Scattered Light," *Physical Review E*, vol. 76, no. 3, 2007.

14. J. Ripoll and V. Ntziachristos, "Quantitative Point Source Photoacoustic Inversion Formulas for Scattering and Absorbing Media," *Physical Review E*, vol. 71, no. 3, 2005.

15. D.A. Schurig, G. Klunder, M. Shannon, R. Russo, and R. Silva, "Signal Analysis of Transients in Pulsed Photoacoustic Spectroscopy," *Review of Scientific Instruments*, vol. 64, no. 2, 1993, pp. 363–373.

16. L.A. Jiang, M. Albota, R. Haupt, J. Chen, and R. Marino, "Laser Vibrometry from a Moving Ground Vehicle," *Applied Optics*, vol. 50, no. 15, 2011, pp. 2263–2273.

17. W.M. Telford, L.P. Geldart, R.E. Sheriff, and D.A. Keys, *Applied Geophysics*. Cambridge, U.K.: Cambridge University, 1990.

18. Laser Institute of America, "ANSI Z136.1—2007," 2007, available at https://www.lia.org/store/product/ansi-z1361-2014-safe-use-lasers-electronic-version.

19. X. Zhang, J.R. Fincke, and B.W. Anthony, "Single Element Ultrasonic Imaging of Limb Geometry: An In-Vivo Study with Comparison to MRI," paper in *Proceedings of the Society of Photo-optical Instrumentation Engineers (SPIE)*, vol. 9790, 2016.

20. R. Haupt, X. Zhang, J. Fincke, J. Richardson, J. Hughes, B. Anthony, and A. Samir, "Non-Contact Laser Ultrasound System for Medical Imaging and Elastography," paper in *Proceedings of IEEE International Ultrasonics Symposium*, 2019, pp. 1921–1925.

21. X. Zhang, J.R. Fincke, C.M. Wynn, M.R. Johnson, R.W. Haupt, and B.W. Anthony, "Full Noncontact Laser Ultrasound: First Human Data," *Nature—Light: Science and Applications*, vol. 8, no. 119, 2019.

22. R. Haupt and A. Samir, "Non-Contact Laser Ultrasound for Biomedical Applications," paper presented at American Institute of Ultrasound in Medicine (AIUM), Orlando, May 2019.

23. J. Fincke, R. Haupt, C. Wynn, X. Zhang, D. Rivera, and B. Anthony, "Characterization of Laser Ultrasound Source Signals in Biological Tissues," *Journal of Biomedical Optics*, vol. 24, no. 2, 2018, pp. 1–11.

24. R. Haupt, C. Wynn, J. Fincke, X. Zhang, B. Anthony, and A. Samir, "Non-Contact Laser Ultrasound for Medical Imaging and Diagnosis," paper in *Proceedings of the IEEE International Ultrasonics Symposium*, 2017.

25. R. Sheriff, *Encyclopedic Dictionary of Exploration Geophysics*. Tulsa: Society of Exploration Geophysicists, 1999.

Appendix

Photoacoustic Phenomenology and Ultrasonic Wave Propagation

Optical Absorption Process

In the first stage of the photoacoustic process, photons are absorbed by particles composing a tissue volume, where the absorption coefficient

$$\mu_a = \rho\,\sigma_a \text{ where }, \sigma_a = -4\frac{2\pi a}{\lambda}\pi a^2 Im\left\{\frac{n_1 - n_0}{n_1 + 2n_0}\right\}$$

and ρ and σ_a are the particle density and cross-sectional area; a is the particle radius, where a is orders of magnitude less than the optical wavelength; and n_1 and n_0 are the refraction indices of the absorbing material and an infinite homogeneous nonabsorbing medium.

For an optical pulse incident on tissue particles, the total absorbed energy, E_a, becomes

$$E_a(\mathbf{r},t) = \mu_a \int_{4\pi} I(\mathbf{r},t,\hat{\mathbf{s}})\,d\Omega = \mu_a U^{inc}(\mathbf{r},t)$$

where I is the specific intensity absorbed by the tissue particles at a position $\mathbf{r}$ from light incident in a direction $\hat{\mathbf{s}}$. U^{inc} is the average incident intensity with units of joules/square centimeter (J/cm^2). The governing relationship establishing tissue deformation, and thus acoustic or elastic wave generation, evolves from the tissue temperature increase caused by the absorbed energy where

$$\rho_m C \frac{\partial T(\mathbf{r},t)}{\partial t} - \kappa\nabla^2 T(\mathbf{r},t) = E_a(\mathbf{r},t)$$

and ρ_m, C, κ, T are the tissue mass density, specific heat, thermal conductivity, and temperature, respectively. The first term in the above equation describes the temperature increase due to optical absorption and diffusion. The optical diffusion is several orders of magnitude larger than the thermal diffusion; thus, the second term in the equation is negligible.

Optical Propagation Process

The next critical component to understanding the process of photoacoustic phenomenology is the effect of optical propagation into a scattering media such as complex biological tissue. The materials composing a tissue mass are considerably heterogeneous. Blood hemoglobin, for example, is highly absorptive, while other tissue cells are highly reflective for wavelengths on the order of 800 nanometers (a commonly used optical wavelength in photoacoustic tomography). However, optical wavelengths greater than 1000 nanometers are strongly absorbed and less sensitive to tissue property variations. The average incident energy can be derived by showing the relationship between the incident energy density in the time domain, where

$$U^{inc}(\mathbf{r_s},\mathbf{r},t) = \frac{S_0}{\left(4\pi Dct\right)^{3/2}}\exp\left[\frac{\left|\mathbf{r_s}-\mathbf{r}\right|}{4Dct} - \mu_a\left|\mathbf{r_s}-\mathbf{r}\right|\right]$$

Optical Conversion to Ultrasound Wave Propagation

Explained next is the last critical component in describing the photoacoustic conversion of light to pressure and the resultant acoustic wave propagation. It is the acoustic or elastic wave that can be measured by an optical receiver such as a laser Doppler vibrometer or conventional contact transducer. For simplicity, we consider the case of an inviscid fluid to demonstrate the generation and propagation of the longitudinal or compressional wave from incident light. We start with the linear force equation

$$\rho_m \frac{\partial^2 \mathbf{u}(\mathbf{r},t)}{\partial t^2} = -\nabla p(\mathbf{r},t)$$

where $\mathbf{u}$ is the acoustic displacement, and p is the acoustic pressure. The relationship between the heat source and the

resultant pressure is shown below in terms of the optical average intensity and optical absorption coefficient:

$$\nabla^2 p(\mathbf{r},t) - \frac{1}{v_s^2}\frac{\partial^2 p(\mathbf{r},t)}{\partial t^2} = \frac{\beta}{C}\Big[\mu_a + \nabla\mu_a(r)\Big]\frac{\partial U(\mathbf{r},t)}{\partial t}$$

The pressure distribution along the tissue column resolves to

$$p(\mathbf{r},t) = p_0(\mathbf{r},t) + \frac{\beta}{4\pi C}\int_V \frac{\mathbf{dr'}}{|r-r'|}\Delta\mu_a(\mathbf{r'})\times$$

$$\left|\frac{\partial U^{inc}(\mathbf{r'},t')}{\partial t'}\right|_{t'=t-|\mathbf{r}-\mathbf{r'}|/v_s}$$

where $p_0(\mathbf{r},t)$ is the incident pressure at the onset of the tissue column

$$p_0(\mathbf{r},t) = \frac{\beta\mu_a}{4\pi C}\int_V \frac{\mathbf{dr'}}{|r-r'|}\left|\frac{\partial U^{inc}(\mathbf{r'},t')}{\partial t'}\right|_{t'=t-|\mathbf{r}-\mathbf{r'}|/v_s}$$

About the Authors

Robert W. Haupt is a senior technical staff member in the Active Optical Systems Group at Lincoln Laboratory. His research emphasis is on coherent laser radar for imaging vibration and acoustic fields and for determining the material properties of biological tissue from a standoff distance. He has developed new system concepts, including the noncontact laser ultrasound for medical imaging, photoacoustic sensing of explosives, buried landmine detection, and seismic cloaking. He is the principal investigator (along with Charles Wynn) and the program manager of the N-CLUS project, which is now funded by the U.S. Army. He has a master's degree in geophysics from the Pennsylvania State University and a master's degree in mechanical engineering from Thayer School of Engineering at Dartmouth College in Hanover, New Hampshire. He has a bachelor's degree in physics and a bachelor's degree in meteorology from the State University of New York at Oswego.

Charles M. Wynn is a technical staff member in the Advanced Capabilities and Technologies Group at Lincoln Laboratory. He is currently leading several photoacoustics efforts and a hyperspectral imaging program. Much of his research in recent years has been on the laser-based detection of trace explosives. He is also engaged in research using photoacoustic spectroscopy for chemical detection and has spearheaded a biotechnology initiative that leverages a novel method for photoacoustic sensing. Most recently, he developed an ultra-compact hyperspectral imager by using computational imaging techniques. He is currently using photoacoustics to create useful audio that can be listened to from a distance. He earned a bachelor's degree in physics from the University of Connecticut, a master's degree in physics from Carnegie Mellon University, and a doctoral degree in physics from Clark University.

Matthew R. Johnson is an associate staff member in the Human Health and Performance Systems Group at Lincoln Laboratory. His work centers on the development of technology for national security and health care, with a specific focus on applying defense technology to the health care sector. He completed his undergraduate studies in electrical engineering at Colorado State University and has completed his MS degree in electrical engineering at MIT.

Jonathan R. Fincke is a research scientist at Phillips Ultrasound in the Boston area and has engaged in research for the development of systems and algorithms for noncontact quantitative ultrasound imaging of soft tissue and bone. He received a bachelor's degree in mechanical engineering from the University of New Hampshire, a master's degree in oceanographic engineering from the MIT/Woods Hole Oceanographic Institution Joint Program, and a doctoral degree in mechanical engineering from MIT.

Xiang Zhang is a postdoctoral scientist in the Department of Mechanical Engineering at MIT. He has engaged in research focusing on the design of electromechanical systems to enhance medical ultrasound, 3D tomographic ultrasound for tissue property characterization, and noncontact laser ultrasound. He received a bachelor's degree in mechanical engineering from the University of Maryland–College Park. During his undergraduate studies, he completed a co-op at the National Institute of Standards and Technology. He holds master's and doctoral degrees from MIT.

Brian W. Anthony is a principal research scientist at the Department of Mechanical Engineering and the Institute for Medical Engineering and Science at MIT. Currently, he is a co-director of the Medical Electronic Device Realization Center and the director of the MIT Master of Engineering in Manufacturing program. His research includes the development of instrumentation and measurement solutions for manufacturing systems, medical diagnostics, and imaging systems.

Anthony E. Samir is an abdominal and interventional radiologist and sonologist at Massachusetts General Hospital. He has a background in medical device innovation. His research interest is in translational applications and technical improvements in ultrasound with a focus on shear wave elastography and tissue characterization. He has expertise in the development, validation, and translation of quantitative imaging biomarkers with ultrasound. He has led numerous projects in liver imaging and in breast imaging. He received an MD degree from University of the Witwatersrand, Johannesburg, Gauteng, and a master's degree in public health from the Harvard School of Public Health.